Summary of the 2012/2013 Asian Winter Monsoon

Northern East Asia, especially the area from eastern Mongolia to northeastern China, experienced cold winter conditions in 2012/2013 as it did in winter 2011/2012. This report summarizes the characteristics of the surface climate and atmospheric/oceanographic considerations related to the Asian winter monsoon for 2012/2013 with focus on the cold conditions observed.

Note: JRA/JCDAS (Onogi et al. 2007) atmospheric circulation data and COBE-SST (JMA 2006) sea surface temperature (SST)/sea ice concentration data were used for this investigation. The outgoing longwave radiation (OLR) data referenced to infer tropical convective activity were originally provided by NOAA. The base period for the normal is 1981 – 2010. The term "anomaly" as used in this report refers to deviation from the normal.

1. Surface climate conditions

In winter 2012/2013, temperatures were lower than normal in northern Asian countries and higher than normal in southern Asian countries and eastern Siberia (Figure 10). Temperatures were 6°C below normal from the southern part of central Siberia to northeastern Kazakhstan in December and around the northern part of eastern Siberia in February.

Figure 11 shows extreme climate events that occurred from December 2012 to February 2013. In December, extremely high temperatures were observed from the Philippines to southern India, and extremely low temperatures were observed from western Japan to Kazakhstan. Figure 12 shows daily temperatures at Shenyang in China and Ulaanbaatar in Mongolia. Daily mean temperatures were below normal throughout most of the winter at Shenyang and during the whole winter except the second half of January at Ulaanbaatar. In January and February, extremely high temperatures were observed in southern Asian countries.

In December, it was reported that a cold wave caused more than 130 fatalities in India and more than 70 in Bangladesh (EM-DAT). The Philippine Government also reported that Typhoon Bopha caused more than 1,000 fatalities in the country in early December 2012.

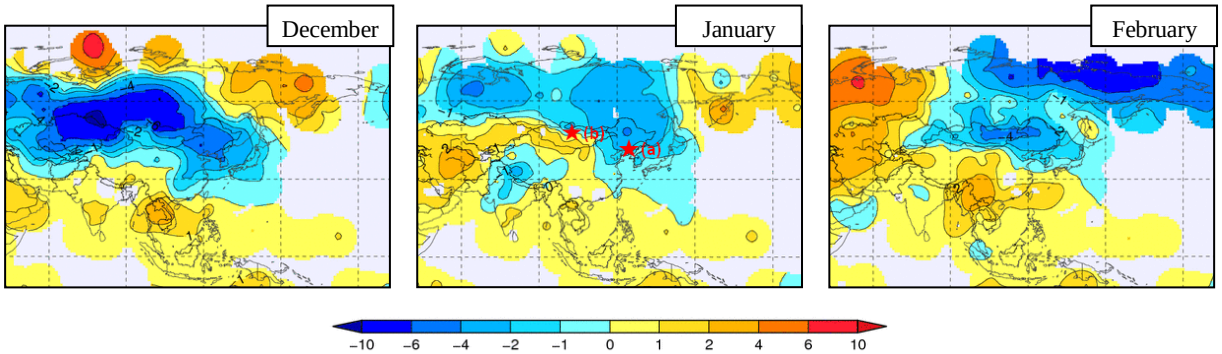

Figure 10 Monthly mean temperature anomalies from December 2012 to February 2013
Anomalies are deviations from the normal (i.e., the 1981 – 2010 average). Daily temperature data for (a) Shenyang (China) and (b) Ulaanbaatar (Mongolia) on the maps are shown in Figure 12.

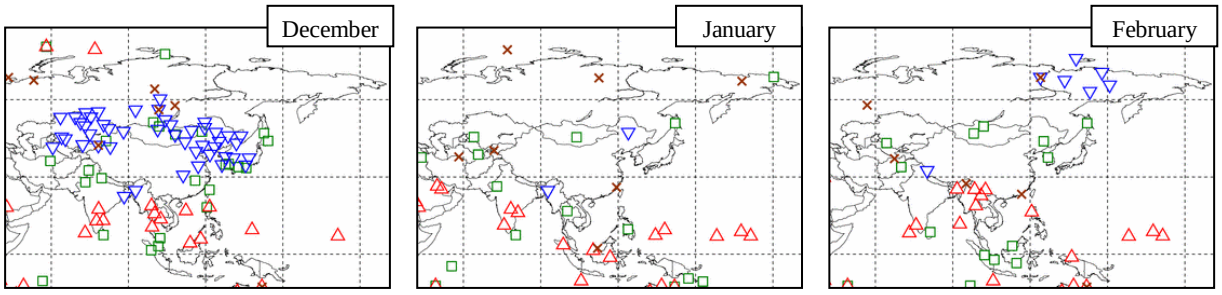

Figure 11 Extreme climate events from December 2012 to February 2013

△ Extremely high temperature (ΔT/SD ≥ 1.83)　□ Extremely heavy precipitation (Rd = 6)

▽ Extremely low temperature (ΔT/SD ≤ -1.83)　× Extremely light precipitation (Rd = 0)

ΔT, SD and Rd indicate temperature anomaly, standard deviation and quintile, respectively.

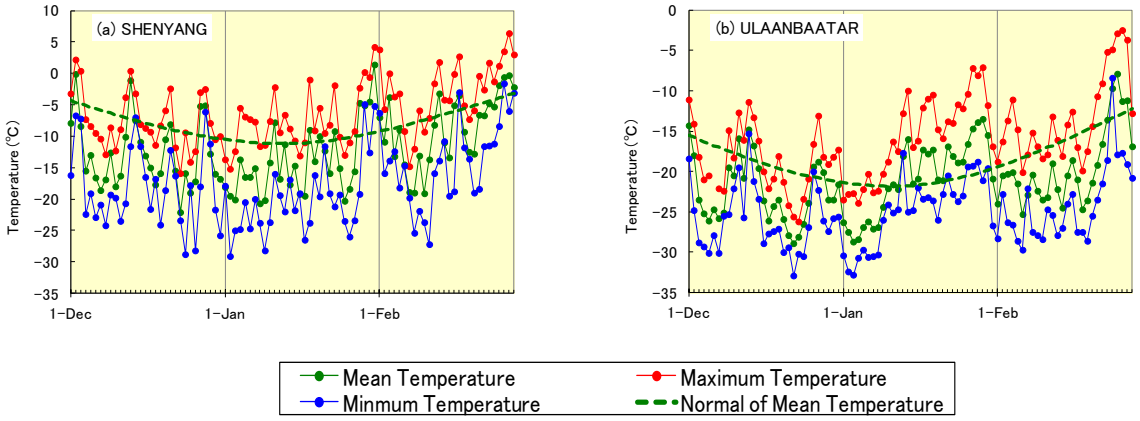

Figure 12 Daily maximum, mean and minimum temperatures (°C) at Shenyang in China and Ulaanbaatar in Mongolia from December 2012 to February 2013 (based on SYNOP reports)

2. Characteristic atmospheric circulation causing cold winter conditions

In winter 2012/2013, sea surface temperatures (SSTs) in the central and eastern equatorial Pacific were below normal, but no La Niña event occurred (Figure 13). SST anomalies indicated warm conditions in the Indian Ocean and the western tropical Pacific, and were significantly above normal in the eastern Indian Ocean and around the Maritime Continent. In line with the enhanced convective activity observed around the eastern Indian Ocean (Figure 14), divergence anomalies were seen there in the upper troposphere (Figure 15 (a)). Wave trains were observed along the Asian jet stream with upper-level anticyclonic and cyclonic circulation anomalies around southern China and over the area to the east of Japan, respectively (Figure 15 (b)).

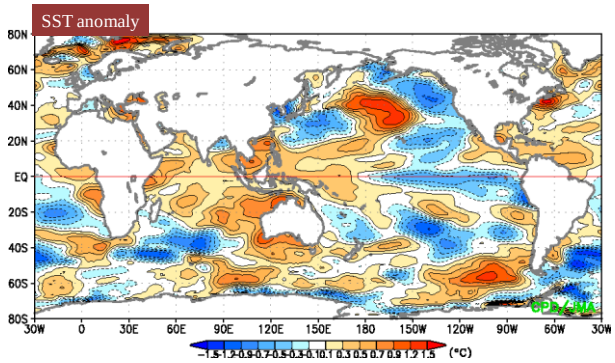

Figure 13 Three-month mean sea surface temperature (SST) anomalies for December 2012 – February 2013

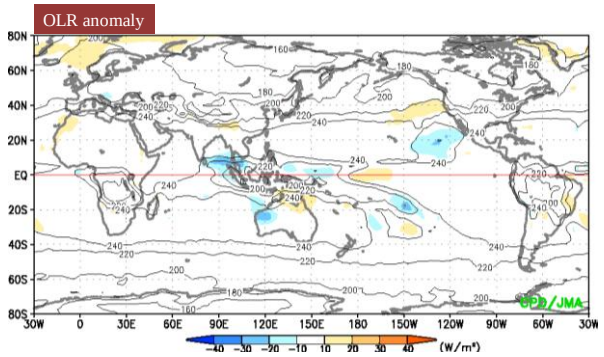

Figure 14 Three-month mean outgoing longwave radiation (OLR) anomalies for December 2012 – February 2013

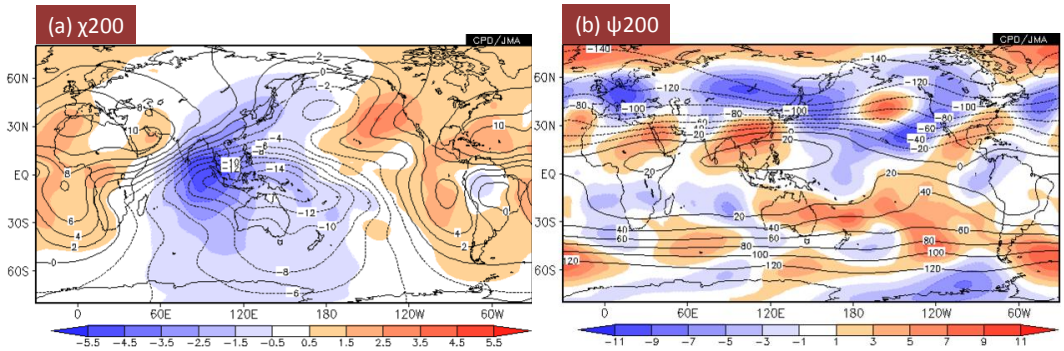

Figure 15 Three-month mean 200-hPa velocity potential and stream function for December 2012 – February 2013
(a) The contours indicate velocity potential at intervals of 2×10^6 m^2/s, and the shading shows related anomalies. (b) The contours indicate the stream function at intervals of 20×10^6 m^2/s, and the shading shows related anomalies.

In the Northern Hemisphere, atmospheric circulation observed during winter featured annular patterns with positive anomalies over the Arctic region and negative anomalies over the mid-latitudes in the troposphere and the stratosphere, indicating negative Arctic Oscillation (AO)-like conditions (Figures 16 (a) – (d)). In association, the polar-front jet stream was generally shifted southward of its normal position over the North Atlantic and Eurasia (Figure 16 (e)), and temperatures in the lower troposphere were below normal over most parts of the Eurasian mid- and high latitudes (Figure 16 (f)).

On the 310-K isentropic surface approximately corresponding to 300-hPa geopotential height in the high latitudes (Figure 17), negative potential vorticity (PV) anomalies were seen over eastern Siberia and the area to the north of Europe, indicating frequent development of blocking highs. Positive PV anomalies were observed from Mongolia to northern Japan in association with blocking flows, indicating frequent movement of split polar vortices with cold air masses toward northern East Asia.

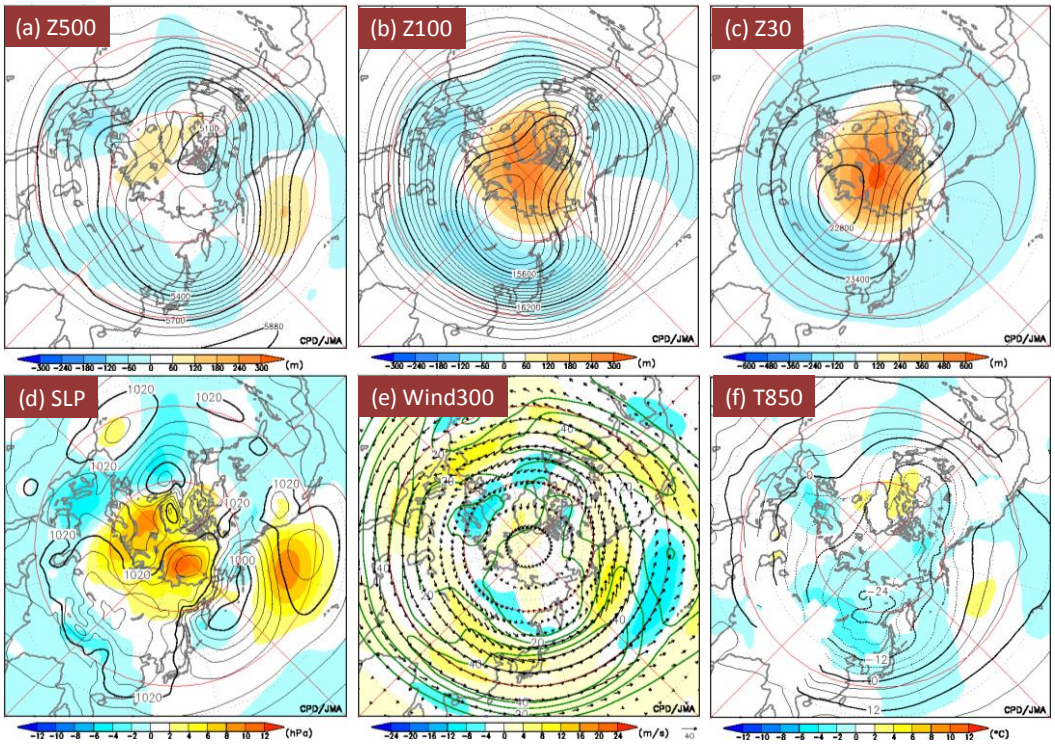

Figure 16 Three-month mean atmospheric circulation in the Northern Hemisphere for December 2012 – February 2013

The contours indicate (a) 500-hPa height, (b) 100-hPa height, (c) 30-hPa height, (d) sea level pressure, (e) 300-hPa wind, and (f) 850-hPa temperature at intervals of 60 m, 60 m, 120 m, 4 hPa, 10 m/s and 4˚C, respectively. The shading indicates related anomalies.

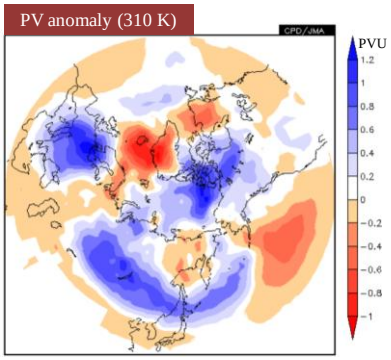

Figure 17 Three-month mean potential vorticity anomalies on the 310-K isentropic surface in the Northern Hemisphere for December 2012 – February 2013

In the stratosphere, the polar vortex remained weak during winter (Figure 18), especially in January 2013 when a major stratospheric sudden warming event occurred (Figure 19). Prevailing planetary wave packets propagated from the troposphere to the stratosphere during December and January (Figure 20 (b)). In association, the polar night jet stream remained weaker than normal during winter (Figure 20 (a)). Easterly wind anomalies in the stratosphere (shown with blue shading in Figure 20 (a)) exhibited peaks with a lag of several days behind the enhancement of upward wave propagation from the troposphere (shown as peaks with red shading in Figure 20 (b)), and easterly anomalies in turn frequently extended from the stratosphere to the troposphere.

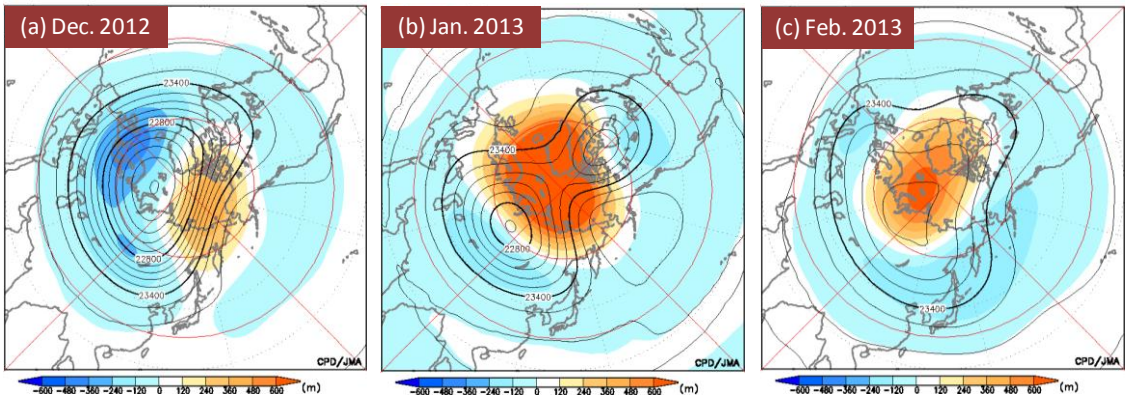

Figure 18 Monthly mean 30-hPa height for (a) December 2013, (b) January 2013 and (c) February 2013
The contours indicate 30-hPa height at intervals of 120 m, and the shading shows related anomalies.

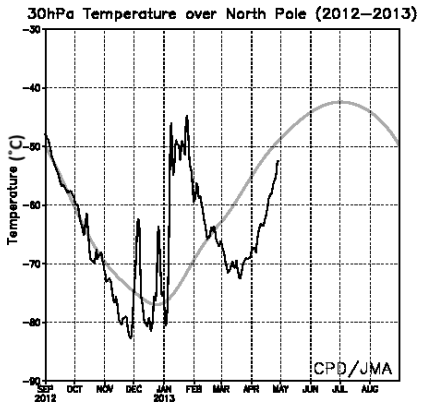

Figure 19 Time-series representation of temperatures at the 30-hPa level over the North Pole (September 2012 – April 2013)
The black line shows daily temperatures, and the gray line indicates the climatological mean.

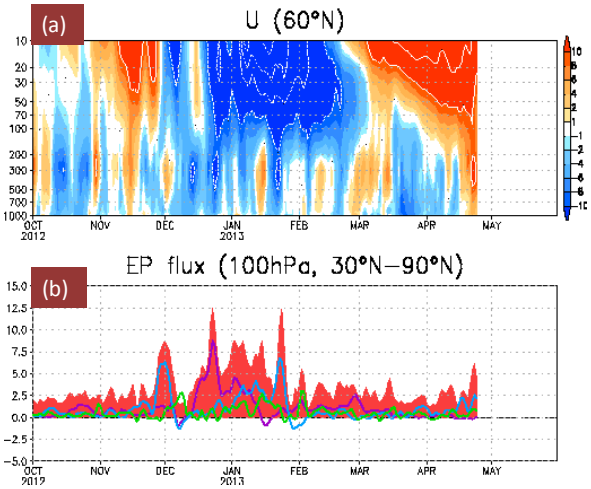

Figure 20 (a) Time-height cross section of zonal mean zonal wind anomalies (m/s) at 60°N, and (b) time-series representation of vertical components of EP flux averaged over 30°N – 90°N at the 100-hPa level (October 2012 – April 2013)
The shading in (a) indicates zonal mean zonal wind anomalies. The red bars in (b) denote the vertical component of EP flux for whole zonal wave numbers. The purple, light-blue and light-green lines denote the vertical components of EP flux for zonal wavenumbers 1, 2 and 3, respectively. The unit for the vertical component of EP flux is m^2/s^2.

3. Primary factors

3.1 Arctic sea ice and high SSTs

During winter 2012/2013, the sea ice extent in the Arctic Ocean remained far below the 1979 – 2000 average, especially in the Barents Sea and the Kara Sea (Figure 21). According to statistical analysis (Figure 22), atmospheric circulation anomalies over Eurasia seen with light sea ice coverage around these seas echoed related anomalies observed during winter (Figure 16), although areas of high sea level pressure with statistical confidence were seen over southern Siberia (Figure 22 (b)) while the anomalies observed were seen over the northern part. Recent studies (e.g., Honda et al. 2009, Inoue et al. 2012) have reported that a reduction in the amount of floating sea ice tends to induce amplification of the Siberian High, leading to cold anomalies in East Asia.

Assessment to determine how SST and sea ice anomalies influence atmospheric circulation was implemented using the atmospheric general circulation model (AGCM) of the Japan Meteorological Agency's one-month prediction model (JMA 2013). The results showed that atmospheric circulation in connection with global SST and sea ice conditions for winter (Figure 23) resembled cold-season conditions (Figure 16) featuring negative AO-like patterns, blocking ridges around eastern Siberia and troughs over northern East Asia. The results of a large ensemble of experiments performed by Deser et al. (2007) using the AGCM showed that high SSTs and light sea ice extents in the North Atlantic sector can force the hemispheric North Atlantic Oscillation-Northern Annular Mode (NAO-NAM) pattern.

Thus, the light sea ice coverage observed around the Barents Sea and the Kara Sea and high SSTs in the Arctic region and the northern North Atlantic may have contributed to the development of negative AO patterns and blocking highs, and consequently the enhancement of the Siberian High.

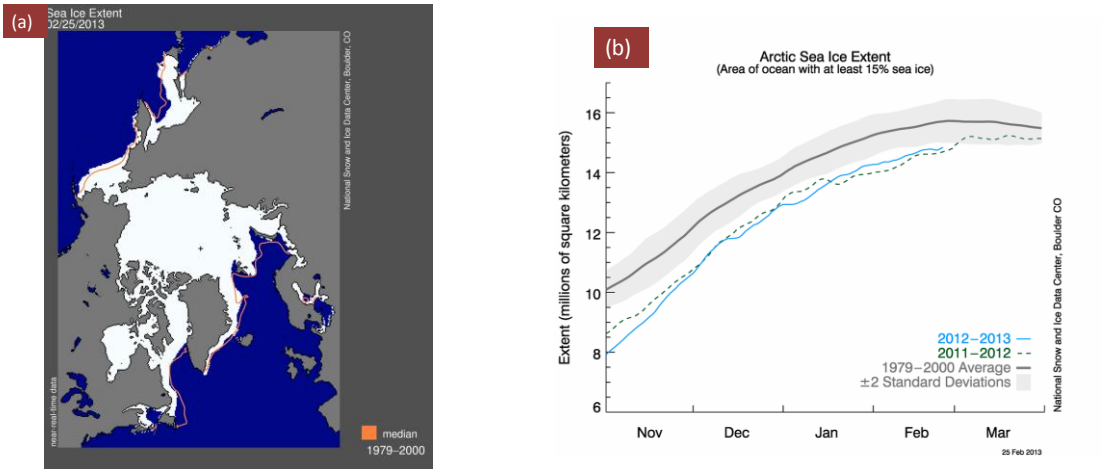

Figure 21 Arctic sea ice extent for winter 2012/2013

(a) Arctic sea ice extent as of 25 February, 2013. The orange line shows the 1979 to 2000 median extent for that month, and the black cross marks the geographic North Pole. (b) Daily Arctic sea ice extent as of 25 February, 2012, along with the corresponding values for the previous year. The current year is shown in light blue, and 2011 – 2012 is shown in dashed green. The gray area around the average line shows the two-standard-deviation range of the data.

(Sources: National Snow and Ice Data Center (NSIDC), USA, at http://nsidc.org/arcticseaicenews/)

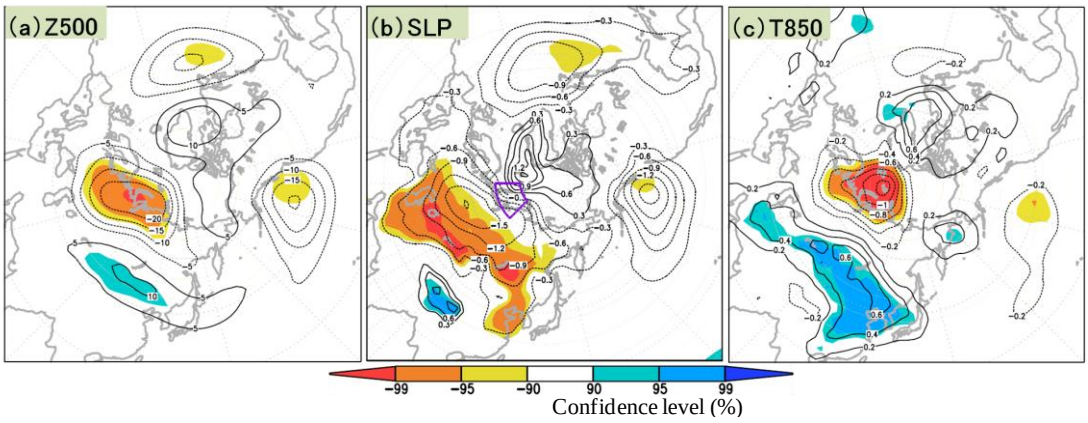

Figure 22 Three-month mean (a) 500-hPa height, (b) sea level pressure, and (c) 850-hPa temperature regressed onto area-averaged sea ice extents around the Barents Sea and the Kara Sea (70˚N – 80˚N, 45˚E – 90˚E) for winters (December – February) from 1979/1980 to 2010/2011

The contour intervals are (a) 5 m, (b) 0.3 hPa, and (c) 0.2˚C. The shading indicates confidence levels as indicated by t-testing. Long-term trends were removed from the datasets before statistical analysis was performed.

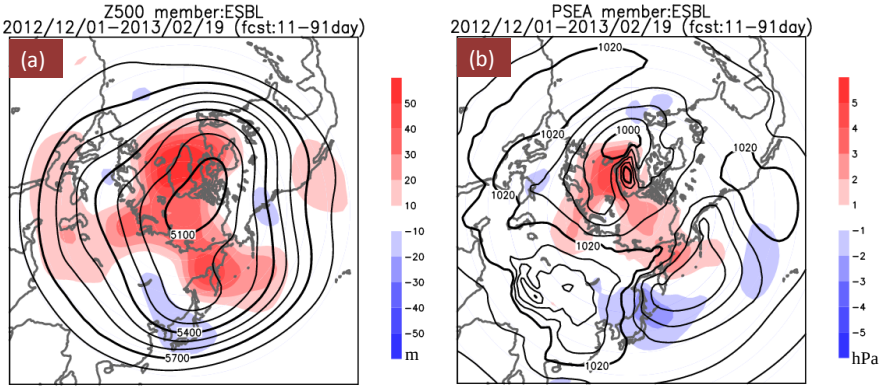

Figure 23 Impacts of sea surface temperature and sea ice anomalies on atmospheric circulation for winter 2012/2013

(a) shows responses of the 500-hPa height to global sea surface temperature (SST) and sea ice anomalies based on output from the Japan Meteorological Agency one-month prediction model (atmospheric general circulation model). In this experiment, 11 members of the model were run and forced with real and normal conditions of daily SST and sea ice. The contours indicate ensemble-mean responses to actual conditions, which are those averaged from 1 December, 2012, to 19 February, 2013. The shading shows deviations between ensemble-mean responses to actual conditions and those to the normal. (b) As per (a), but for sea level pressure at contour intervals of 5 hPa.

3.2 Troposphere-stratosphere interaction

Planetary wave packets of zonal wavenumber 2 propagated upward in the mid-latitudes of the Northern Hemisphere, reflected around the tropopause, turned northward, and converged in the upper troposphere of the high latitudes (Figure 24 (a)). Divergence and convergence of EP flux lead to acceleration and deceleration of westerly winds. As a result, northward wave propagation from mid- to high latitudes contributed to the development of negative AO-like conditions. The path of the wave propagation was consistent with the distribution of the refractive index related to the vertical profile of mean westerly winds (Figure 24 (b)). The vertical profile of westerly winds may have been affected by dominant wave propagation originating in the mid-latitudes.

Thus, it can be hypothesized that interaction between the troposphere and the stratosphere may have contributed to negative AO-like patterns, although further investigation is needed.

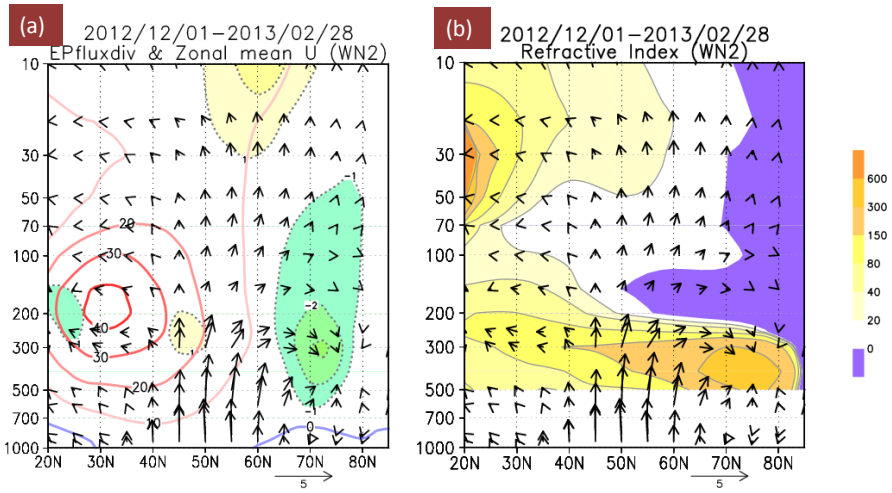

Figure 24 Latitude-height cross section of zonally averaged zonal wind, EP flux and the refractive index for winter 2012/2013

The vectors indicate EP flux for zonal wavenumber 2 in both (a) and (b). (a) The solid contours show zonal wind at intervals of 10 m/s. The shading and dashed contours denote divergence (yellow: positive values) and convergence (negative values) of EP flux at intervals of 1 m/s/day (zero not shown). (b) The shading indicates the refractive index. Wave packets can propagate only in areas with positive index values, and areas with high values act as waveguides.

3.3 Tropical convection and SSTs

The results of AGCM experiments forced with global SST anomalies show upper-level divergence anomalies around the eastern Indian Ocean and anticyclonic and cyclonic circulation anomalies over southern Asia and Japan, respectively (Figure 25). These anomaly patterns resemble those observed for winter (Figure 15). The results of linear baroclinic model experiments forced with convective heating anomalies over the eastern Indian Ocean also show such upper-level circulation anomaly patterns (Figure 26). It can therefore be presumed that enhanced convective activity around the eastern Indian Ocean in association with high SSTs contributed to southward meandering of the jet stream near Japan.

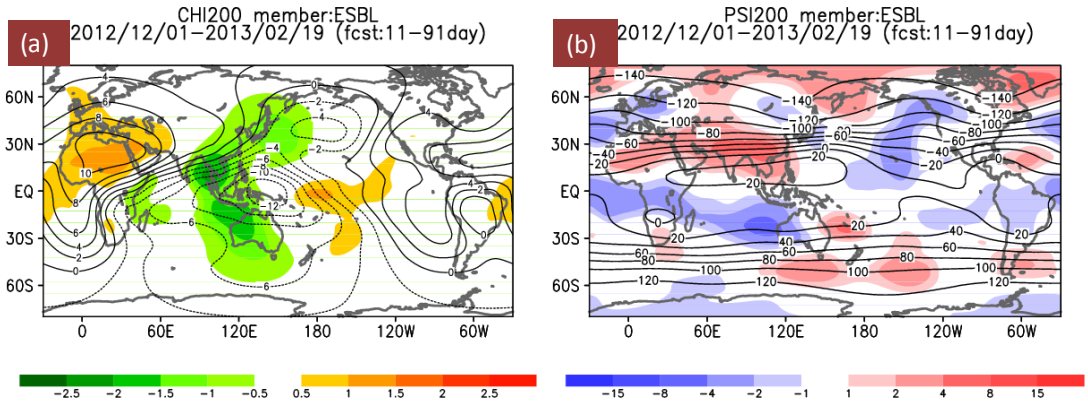

Figure 25 Impacts of sea surface temperature and sea ice anomalies on atmospheric circulation in the upper troposphere for winter 2012/2013

As per 23, but (a) for 200-hPa velocity potential at contour intervals of 2×10^6 m^2/s, and (b) for the 200-hPa stream function at contour intervals of 20×10^6 m^2/s.

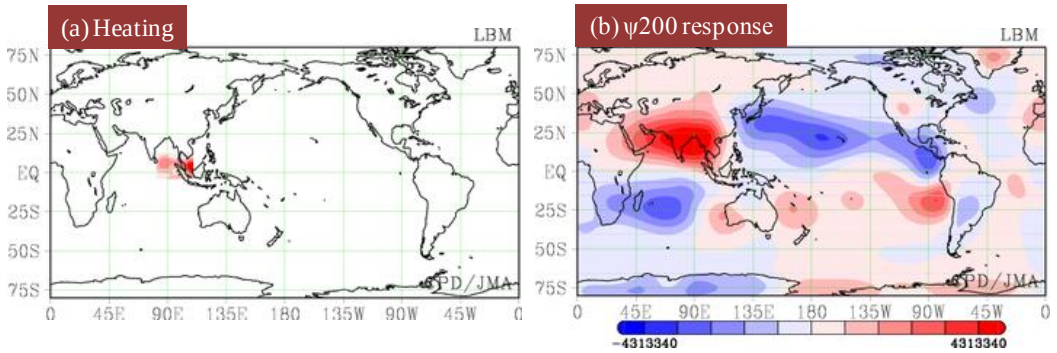

Figure 26 Steady response in a linear baroclinic model (LBM) to heating anomalies around the eastern Indian Ocean for winter 2012/2013

(a) The red shading indicates diabatic heating for the LBM with the basic state for December-January-February (i.e., the 1981 – 2010 average based on JRA-25 data). (b) The shading denotes the steady response of 200-hPa stream function anomalies (m^2/s). These anomalies as responses represent deviations from the basic states, and are additionally subtracted from the zonal averages of the anomalies.

4. Summary

In the 2012/2013 Asian winter monsoon season, northern East Asia experienced a cold winter in association with negative AO-like conditions and blocking patterns around eastern Siberia. The characteristic atmospheric circulation causing the cold conditions may have been related to high SSTs and light sea ice coverage in the Arctic region, troposphere-stratosphere interaction, and enhanced convection around the eastern Indian Ocean. The possible primary factors contributing to these conditions are summarized in Figure 27, but the related mechanisms have not yet been fully clarified.

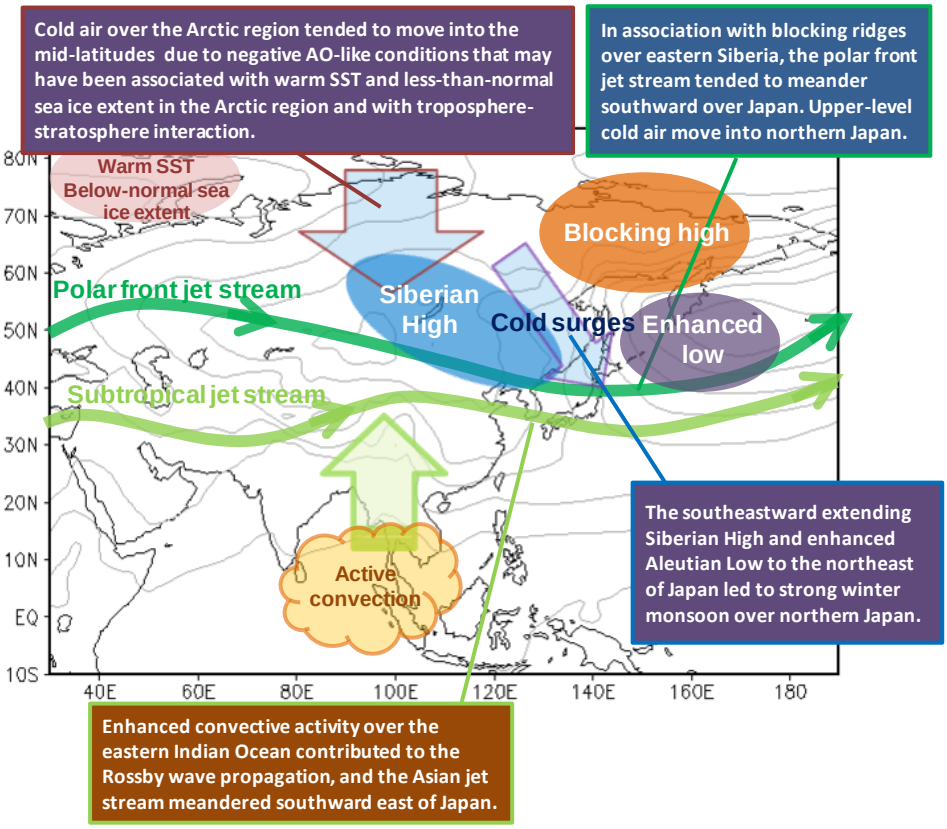

Figure 27 Primary factors contributing to cold 2012/2013 winter conditions in East Asia

References

Deser, C., R. A. Tomas, and S. Peng, 2007: The transient atmospheric circulation response to North Atlantic SST and sea ice anomalies. *J. Climate*, **20**, 4751 – 4767.

Honda, M., J. Inoue, and S. Yamane, 2009: Influence of low Arctic sea-ice minima on anomalously cold Eurasian winters. *Geophys. Res. Lett.*, **36**.

Inoue, J., M. Hori, and K. Takaya, 2012: The Role of Barents Sea Ice in the Wintertime Cyclone Track and Emergence of a Warm-Arctic Cold-Siberian Anomaly. *J. Climate*, **25**, 2561 – 2568.

JMA, 2006: Characteristics of Global Sea Surface Temperature Data (COBE-SST), *Monthly Report on Climate System*, Separated Volume No. **12**.

JMA, 2013: Outline of the operational numerical weather prediction at the Japan Meteorological Agency. *Appendix to WMO Technical Progress Report on the Global Data-processing and Forecasting System and Numerical Weather Prediction Research*.

Onogi, K., J. Tsutsui, H. Koide, M. Sakamoto, S. Kobayashi, H. Hatsushika, T. Matsumoto, N. Yamazaki, H. Kamahori, K. Takahashi, S. Kadokura, K. Wada, K. Kato, R. Oyama, T. Ose, N. Mannoji and R. Taira, 2007: The JRA-25 Reanalysis. *J. Meteorol. Soc. Japan*, **85**, 369 – 432.